J Solid State Electrochem (2010) 14:1145–1152
DOI 10.1007/s10008-009-0941-z

ORIGINAL PAPER

Electrochemical behavior of Ni-Al-Fe alloys in simulated human body solution

I. E. Castañeda · J. G. Gonzalez-Rodriguez · J. Colin · M. A. Neri-Flores

Received: 25 June 2009 / Revised: 10 September 2009 / Accepted: 16 September 2009 / Published online: 15 October 2009

Abstract An investigation about the corrosion resistance of Ni-Al-Fe intermetallic alloys in simulated human body fluid environments has been carried out using electrochemical techniques. Tested alloys included 57 (wt%) Ni-(20 to 30) Al-(12 to 23) Fe using the Hank's solution because the high corrosion resistance provided by protective Al_2O_3 external layer. For comparison, AISI 316L type stainless steel has also been used. Electrochemical techniques included potentiodynamic polarization curves, electrochemical impedance spectroscopy, and electrochemical noise measurements. The different techniques have shown that these alloys showed a similar or higher corrosion resistance than conventional AISI 316L type stainless steel, and this corrosion resistance decreased as the Al content in the alloy increased. The alloys were susceptible to pitting type of corrosion on the interdendritic Ni-rich phases.

Keywords Corrosion · Human body · Electrochemical impedance · Electrochemical noise

I. E. Castañeda · J. G. Gonzalez-Rodriguez · M. A. Neri-Flores
CIMAV, Complejo Industrial Chihuahua,
Chihuahua, Mexico

J. G. Gonzalez-Rodriguez (✉)
Centro de Investigación en Ingeniería y Ciencias Aplicadas,
UAEM,
Av. Universidad 1001, Col. Chamilpa,
Cuernavaca Mor., Mexico
e-mail: ggonzalez@uaem.mx

J. Colin
Facultad de Ciencias Quimicas e Ingeniería, UAEM,
Av. Universidad 1001, Col. Chamilpa,
Cuernavaca Mor., Mexico

Introduction

Corrosion of human body metallic implants is critical because it can adversely affect biocompatibility and mechanical integrity [1]. Corrosion and surface film dissolution are two responsible mechanisms for introducing ions in the body from the implants. Extensive release of metal ions from human body implants can result in adverse biological reactions and even lead to mechanical failure of the device. Most of the used materials for human implants include AISI 316L type stainless steels [2, 3], titanium-base alloys [4–8], or cobalt-base alloys [9–13]. Aluminides are receiving a considerable attention relative to aqueous corrosion properties such as acidic, basic, chloride, and sulfur-compound solutions [14–17]. Among the novel room temperature applications of these materials is that they can be considered their potential use such as biomaterials, or in applications in a seawater atmosphere [14–17]. Garcia-Alonso, for instance, found that the corrosion rate of Fe_3 Al-type intermetallic under three different heat treatments were within the same order of magnitude than that for 316L type stainless steel in a simulated human body fluid [14] whereas Lopez [15] obtained similar results with another iron-base alloy.

Nickel aluminide, NiAl, is an intermetallic compound that is formed as a result of the ordering of nickel and aluminum atoms on the face-centered cubic unit cell. As a promising intermetallic, it can be used in both low and high temperature due to its high melting point, low density, and excellent thermal conductivity. They have excellent corrosion resistance in most environments due to the establishment of an external aluminum oxide, Al_2O_3 layer [18]. Ternary additions to Ni-Al have been investigated by several researchers [16–18], and it has been reported, for instance, that Fe additions substitute equally for both Ni and Al. During the solidifica-

tion of Ni-Al alloys with ternary additions of Fe, Co, Cr, or Cu, ternary elements were distributed into γ phase; in particular, Fe additions induced the formation of γ phase [19], and small amounts of Fe destabilized the β phase and induced the β martensite transformation. The resistance to aqueous, low temperature corrosion of Ni-Al alloys should be of concern for high temperature applications because these materials will not always be operating at high temperatures, but they can be used at low temperatures also, and corrosion damage during fabrication or maintenance could lead to catastrophic failures during service. Thus, the goal of this work is to investigate the effect of Fe content alloying a NiAl alloy on its corrosion resistance in human body solutions for potentially biomaterials applications. The solution which most adequately simulates human body environment, and the most widely used, is the called Hank's solution [2–13].

Experimental procedure

Chemical compositions of tested Ni-Al-Fe alloys are given on Table 1. They were induction-melted in vacuum at 1,700 °C and then cast it. For comparison, some tests were performed on an AISI 316L type stainless steel also. To perform the corrosion test experiments, these specimens were polished with diamond paste to a 0.1 μm finish. Electrochemical experiments were performed using an ACM Instruments potentiostat controlled by a personal computer. Potentiodynamic polarization curves were obtained by varying the applied potential from −500 mV with respect to open circuit potential, E_{corr}, up to +600 mV at a scan rate of 1 mV s^{-1}. Corrosion current density values, i_{corr}, were calculated by using the Tafel extrapolation method, which is valid for the sweep rates used here, and taking an extrapolation zone of ±250 mV around the E_{corr} value once it was stable, as shown on Fig. 1. Curves were performed by triplicate. Passive current density value, i_{pp}, was obtained as the average value from three different readings, and the pitting or breakdown potential, E_{pit}, was taken as the potential value where an abrupt increase in the anodic current density was observed. Before running the experiments, the E_{corr} value was measured during approximately 30 min in order to reach a steady-state condition. All potentials were measured using a saturated calomel electrode (SCE) as reference electrode. The counter electrode was a platinum wire with a diameter of 1.00 mm and 15 cm long. Linear polarization resistance measurements were performed by polarizing the specimen from +10 to −10 mV, with respect to E_{corr}, at a scan rate of 1 mV s^{-1} every day during 16 days as an average time. All electrochemical tests were performed at 37±2 °C because that is the human body temperature, which was controlled by using an electric heating mantle where the electrochemical cell was immersed. Electrochemical impedance spectroscopy tests (EIS) were carried out at E_{corr} by using a signal with amplitude of 10 mV peak-to-peak and a frequency interval of 0.1 Hz–30 kHz by taking 200 points per decade. The working area was 1.0 cm^2. Finally, electrochemical noise measurements in both current and potential were recorded using two identical working electrodes and a SCE. The electrochemical noise measurements were made recording simultaneously the potential and current fluctuations at a sampling rate of 1 point per second during a period of 1,024 s. A fully automated zero resistance ammeter from ACM instruments was used in this case. Removal of the DC trend from the raw noise data was the first step in the noise analysis when needed. To accomplish this, a least square fitting method was used. Finally, the noise resistance, R_n, was then calculated as the ratio of the potential noise standard deviation, σ_v, over the current noise standard deviation, σ_i. The aqueous solution used included the Hank's solution with a chemical composition as given on Table 2.

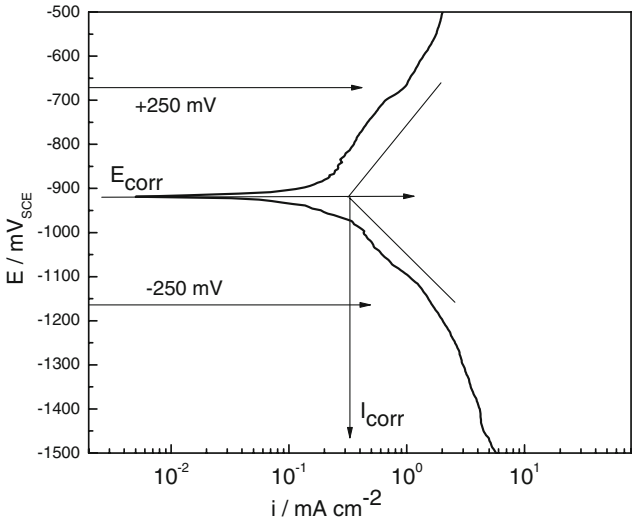

Fig. 1 Scheme showing the procedure to calculate i_{corr} and Tafel slopes

Table 1 Chemical composition of used materials (wt%)

Material	Ni	Al	Fe
b1	57	20	23
b2	57	22.5	20.5
b3	57	25	18
b4	57	27.5	15.5
b5	57	30	13

Results and discussion

Figure 2 shows polarization curves for the different Ni-AL-Fe alloys together with that for AISI 316L type stainless

Table 2 Chemical composition of the Hank's solution

	NaCl	$CaCl_2$	KCl	Glucose	$NaHCO_3$	$MgCl_2.6H_2O$	$Na_2HPO_4.2H_2O$	KH_2PO_4	$MgSO_47H_2O$
g l^{-1}	8	0.14	0.4	1	0.35	1	0.06	0.06	0.06

steel. It can be seen that the curves, in all cases, displayed an active–passive behavior, probably due to the establishment of a mixture of Al_2O_3 and NiO oxides, where the noblest E_{corr} value was for AISI 316L type stainless steel; for the Ni-Al-Fe alloys, the alloy containing 20% Al had the noblest E_{corr} value, around −420 mV_{SCE}, and this value went towards more active values as the Al content increased, reaching a value around −488 mV_{SCE} for the alloy containing 30% Al, noticing a displacement towards the nobler side of about 200 mV_{SCE} by the AISI 316L type stainless steel sample, which is associated with a decrease in the corrosion current density value. The corrosion current density value, i_{corr}, was lowest for AISI 316L type stainless steel, whereas for the Ni-AL-Fe alloys, the lowest i_{corr} value was for the alloy with the lowest Al content, and it increased as the Al content increased. In a similar way, the noblest pitting potential value, E_{pit}, was for AISI 316L type stainless steel, whereas for the intermetallic alloys, it decreased as the Al increased, as well as the primary passive current density value, i_{pp}. All these parameters are summarized on Table 3. Thus, all the evidence shows that the Ni-Al-Fe alloys had lower corrosion properties in a simulated human body environment than the AISI 316L type stainless steel. However, since polarization curves only provide a short time behavior, more information is necessary for longer times evaluation.

The change in the linear polarization resistance value, R_p, with time for the different Ni-Al-Fe alloys and for AISI 316L type stainless steel is given on Fig. 3, where it can be seen that, although during the first hours of testing, the highest R_p value, and thus, the lowest corrosion rate, was for AISI 316L type stainless steel, whereas the Ni-AL-Fe alloy containing 20% Al exhibited similar R_p values to that shown by AISI 316L type stainless steel and remained more or less constant, with a slight tendency to decrease as time elapsed, indicating that this alloy showed a similar corrosion resistance in simulated human body conditions than that shown by AISI 316L type stainless steel. The R_p value for the rest of the Ni-Al-Fe alloys decreased as the Al contents decreased and showed an erratic behavior as time elapsed, indicating the detachment of any formed protective formed layer. This erratic behavior can be due to the formation and detachment of the passive layer, exposing the metal to further attack. It should be noted, however, that during the last 5 days of testing, all the intermetallic alloys showed similar, or even higher R_p values, and thus, lower corrosion rates than that exhibited by AISI 316L type stainless steel.

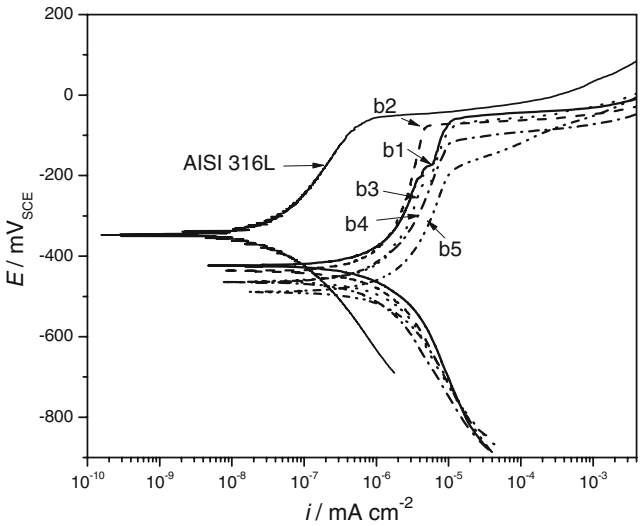

Fig. 2 Effect of Al content on the polarization curves for Ni-AL-Fe intermetallic alloys in Hank's solution

EIS data in the Nyquist format for the different intermetallic alloys are shown on Fig. 4a where it can be seen that, in all cases, the data described one depressed, capacitive-like, semicircle with their centers on the real axis at high frequencies and a second semicircle at intermediate and lower frequency values. The presence of the first semicircle is related to the charge transfer from the metal to the solution through the double electrochemical layer, whereas the second semicircle is due to the presence of a protective, passive layer, probably a mixture of NiO and Al_2O_3 oxides just as evidenced by polarization curves shown on Fig. 2, indicating that the corrosion process was under charge transfer control. In such a process, the semicircle diameter or the charge transfer resistance, R_{ct}, is equivalent to the linear polarization resistance value, R_p.

Table 3 Electrochemical parameters obtained from polarization curves

Material	E_{corr}/mV_{SCE}	i_{corr}/A cm^{-2}	E_{pit}/mV_{SCE}	i_{pp}/A cm^{-2}
b1	−421	4.6 10^{-4}	−62	1.6 10^{-3}
b2	−438	5.7 10^{-4}	−81	1.8 10^{-3}
b3	−461	6.8 10^{-4}	−92	2.4 10^{-3}
b4	−465	7.2 10^{-4}	−118	2.8 10^{-3}
b5	−488	1.2 10^{-3}	−192	4.6 10^{-3}
316L	−347	4.1 10^{-5}	−65	2.1 10^{-4}

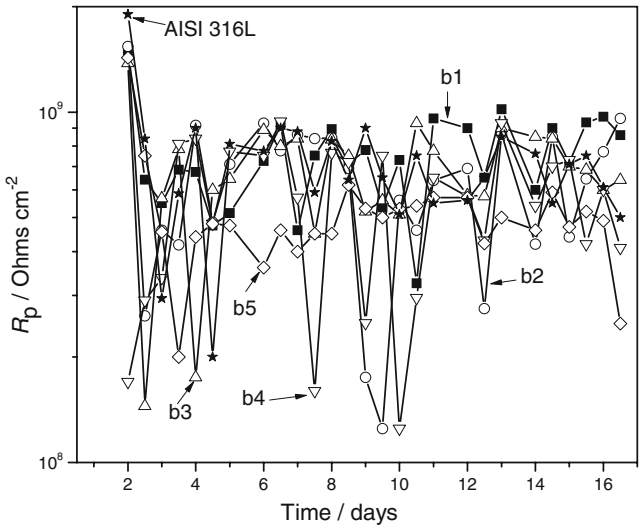

Fig. 3 Effect of Al content on the change in the R_p value with time for Ni-AL-Fe intermetallic alloys in Hank's solution

In the case of intermetallic alloy b1, the one containing 20% Al, the data described a straight line after the low frequency semicircle, indicating that the corrosion process in this particular case was under a mixed charge transfer and diffusion control of the aggressive ions through the protective, passive layer. Bode diagrams shown on Fig. 4b show that the highest impedance modulus was shown by intermetallic b1 (20% Al), whereas the lowest impedance modulus was obtained by intermetallic b5 (30% Al). On the other hand, Bode-phase diagram shown on Fig. 4c shows that in all cases, there are two time constants; a highly capacitive behavior, typical of passive materials, is indicated from medium to low frequencies by phase angles approaching −90°, suggesting that a very stable film is formed on all tested alloys in the used electrolyte. From Fig. 5, it can be seen that the semicircle diameter for intermetallic b2, $R_{ct,}$ did not remain constant with time, instead it showed an erratic behavior. This behavior was similar to that observed by R_p on Fig. 3.

EIS data can be modeled by using the equivalent electric circuit shown on Fig. 6, where R_s represents the solution or electrolyte resistance, R_{po} is the porous layer resistance associated to the charge transfer resistance and C_{po}, its capacitance, and R_b is the resistance of the barrier layer associated to the participation of adsorbed intermediates and C_b, its capacitance. When a nonideal frequency response is present, it is commonly accepted to employ distributed circuit elements in an equivalent circuit. The most widely used is constant phase element (CPE) which has a noninteger power dependence on the frequency. The impedance of a CPE is described by the expression:

$$Z_{CPE} = Y^{-1}(j\omega)^{-n} \quad (1)$$

where Y is a proportional factor, j is $\sqrt{-1}$, ω is the frequency, and $-1<n<1$ has the meaning of a phase shift. Often, a CPE is used in a model in place of a capacitor to compensate for nonhomogeneity in the system. Calculated parameters to simulate the EIS data for different intermetallic alloys are shown on Table 4. It can be seen that the resistance of the barrier layer associated to the participation of adsorbed intermediates, R_b, is, in all cases, significantly higher than the resistance of the porous layer, $R_{po.}$ This

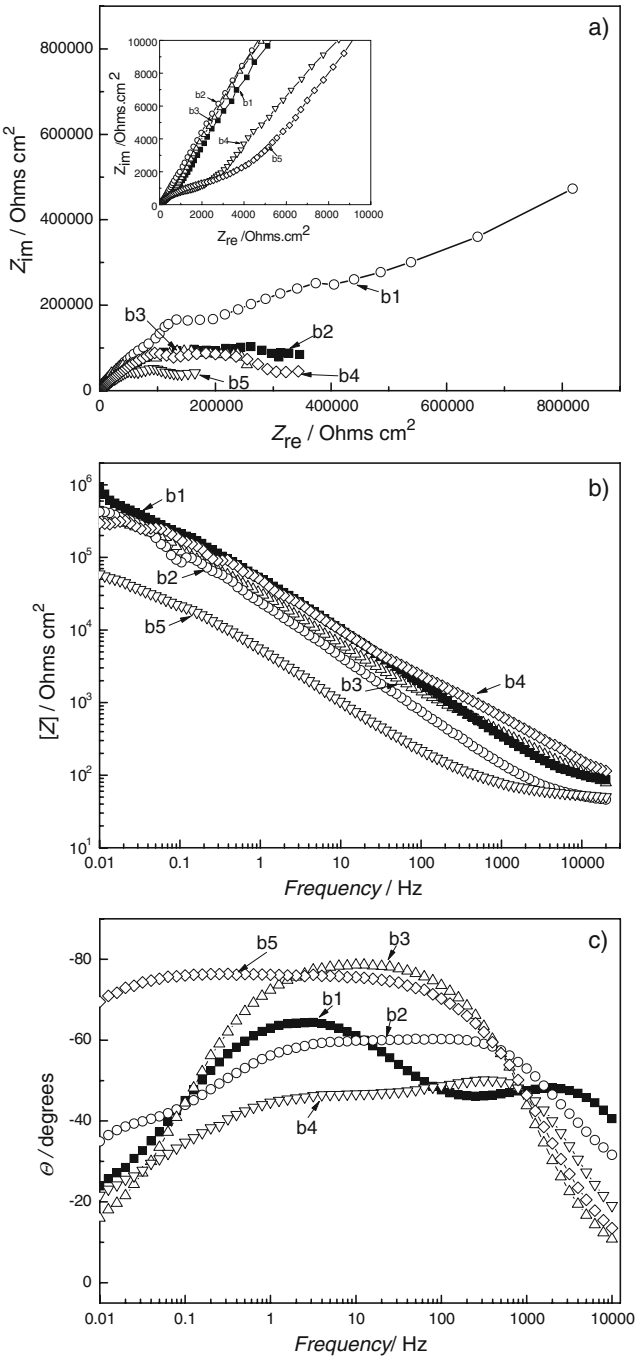

Fig. 4 Effect of Al content on the **a** Nyquist **b** Bode, **c** Bode-phase curves for Ni-Al-Fe intermetallic alloys in Hank's solution

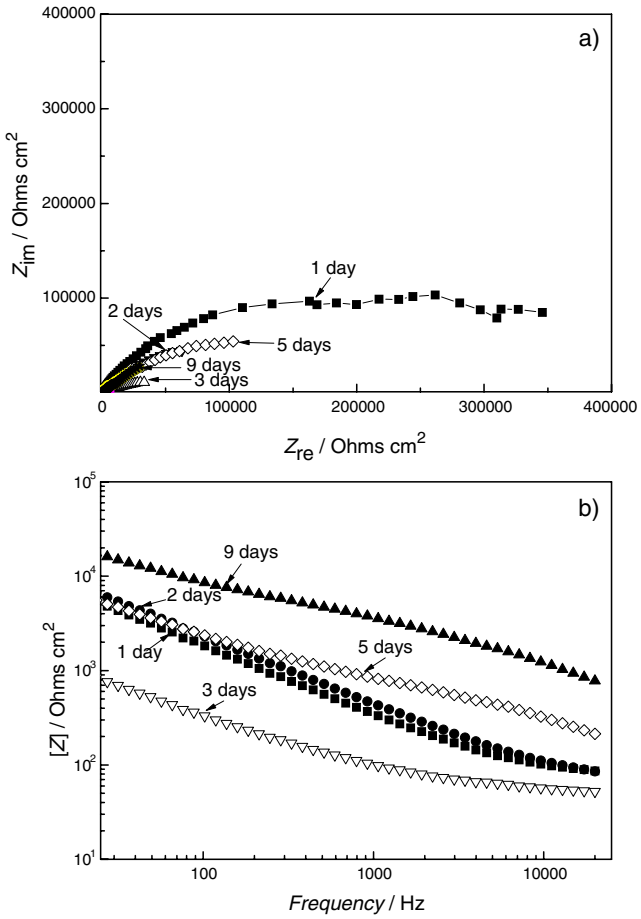

Fig. 5 Change with time on the **a** Nyquist and **b** Bode diagrams for Ni-Al-Fe intermetallic alloy containing 22.5% Al in Hank's solution

indicates that the protection is predominantly given by the inner barrier layer, as also provided in the literature [21–24]. The R_b value for alloy b2, as given on Table 5, showed an erratic behavior during the first days, which means that the film formed by adsorbed intermediates, for instance NiO or Al_2O_3 oxides, increases in thickness and then it decreases after some time. After 7 days or so, this formed film is stabilized as observed by the stable values in R_b, giving values very similar to those obtained by AISI 316L type stainless steel and are responsible for the high corrosion resistance in this environment.

In order to have an insight of the susceptibility of these materials towards a localized type of corrosion, some electrochemical noise measurements in both current and potential were carried out. Examples of these readings for the alloy containing 20% Al are shown on Fig. 7, where it can be seen only transients of very high frequency and small intensity, typical of a material which is in a passive state, combined with a few transients of higher intensity, with an abrupt increase in their intensity and a slow decay, typical of a material undergoing a localized type of corrosion. By using the potential noise standard deviation, σ_v, and dividing it by the current noise standard deviation, σ_i, we can obtain the noise resistance, R_n, and its change with time for the different intermetallic alloys is shown on Fig. 8. It can be seen that, generally speaking, the highest R_n value was for the alloy with the lowest Al content and that it decreased as time elapsed, showing an erratic behavior with time. This erratic behavior was very similar to that exhibited by R_p, Fig. 3, and R_{ct}, Fig. 5, which enables us to say that R_n gives information about the corrosion rate in the same way as R_p does. Thus, by using any analysis tool, alloy b1 showed the highest corrosion resistance. There is a factor called the "localization index, LI" defined as:

$$\mathrm{LI} = \frac{\sigma_i}{i_{rms}} \tag{2}$$

where σ_i is the current noise standard deviation and i_{rms} is the current root mean square [25]. This shows that when the values for LI lie between 1 and 0.1, the alloy is highly susceptible to localized corrosion; when the values for LI lie between 0.1 and 0.01, the alloy is susceptible to a mixture of both uniform and localized corrosion. Finally, when the values for LI lie between 0.01 and 0.001, there is a tendency towards uniform corrosion. Table 6 shows the LI for all alloys were always lied between 1 and 0.1, indicating that they were highly susceptible to a localized type of corrosion, although this susceptibility decreased in a marginal way towards the end of the test.

The above results were confirmed by SEM analysis of the corroded surface of the different specimens. Thus, Fig. 9 shows that the different intermetallic alloys suffered from a localized type of corrosion, where it can be seen that the most susceptible phase to pitting corrosion was the Al-rich interdendritic one, which was more evident on Fig. 10. On these micrographs, the dendritic phase increased in percentage as the Al content increased, which were Al-rich phases, whereas the interdendritic phases were Ni and/or Fe rich. In general terms, it has been shown that the resistance of Ni-Al-Fe type aluminides to uniform corrosion decreased by alloying them with Al. As the Al content increased, the resistance to both uniform and localized corrosion decreased. Thus, interdendritic phases were the most susceptible towards a localized type of corrosion. This can be explained in terms of the galvanic effect, since the Al-rich dendritic phases acted as cathode, whereas the interdendritic phases acted as anodes making them very

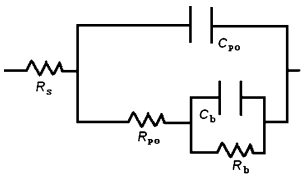

Fig. 6 Equivalent circuit to simulate experimental EIS data

Table 4 Parameters calculated to simulate the EIS data for the different alloys tested

Material	R_s	Y_{po}	n_{po}	R_{po}	Y_b	n_{pb}	R_b
b1	41.25	1.04E−05	0.88491	14839	1.82E−05	0.56601	727658
b2	36.43	6.65E−06	0.69508	282220	1.46E−05	0.70264	689220
b3	39.2	1.14E−05	0.49465	76.65	6.26E−06	0.88482	140180
b4	35.8	5.00E−06	0.10732	887.5	8.44E−06	0.89553	245473
b5	43	5.19E−06	0.8103	712.5	4.16E−05	0.52075	21643
316L	41.13	8.09E−06	0.85686	578.7	1.46E−06	0.84417	9.04E+06

Table 5 Parameters calculated to simulate the EIS data for alloy b2 at different immersion times

Day	R_s	Y_{po}	n_{po}	R_{po}	Y_b	n_{pb}	R_b
1	76.43	6.65E−06	0.69508	282220	1.46E−05	0.70264	689220
2	129.3	7.66E−06	0.62379	720060	2.89E−04	1.44	134870
3	56.27	4.48E−06	0.59963	5369	1.47E−06	0.78028	975480
4	30.57	3.41E−06	0.61045	5408	1.77E−06	0.74024	1.03E+06
5	92.71	6.39E−06	0.68626	309150	9.17E−05	1.046	95466
6	10	2.65E−06	0.60536	7220	2.27E−06	0.81753	969820
7	39.55	3.02E−06	0.58769	7761	1.95E−06	0.84487	1.04E+06
8	124.3	2.09E−06	0.59334	11208	2.23E−06	0.82129	1.47E+06
9	133.2	1.61E−06	0.60861	12890	2.44E−06	0.79883	1.58E+06
10	110.2	1.21E−06	0.6321	14320	2.68E−06	0.75816	2.22E+06
11	170.9	1.37E−06	0.61248	16052	2.33E−06	0.78898	1.85E+06
12	157.6	1.28E−06	0.61881	14905	2.51E−06	0.77666	1.76E+06
13	299.1	2.21E−06	0.55574	20326	1.70E−06	0.8486	1.87E+06
14	331.4	2.42E−06	0.5442	23426	1.54E−06	0.85962	1.95E+06
15	56.3	7.26E−06	0.71588	317950	1.54E−03	4.852	2.79E+05
16	88.16	3.51E−04	0.45491	28.8	3.51E−04	0.45576	6.89E+06

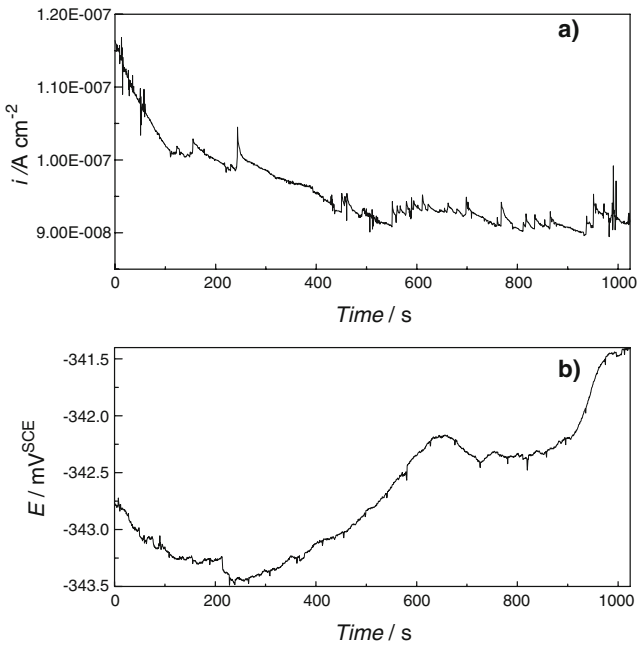

Fig. 7 Noise in **a** current and **b** voltage for Ni-Al-Fe intermetallic alloy containing 22.5% Al in Hank's solution

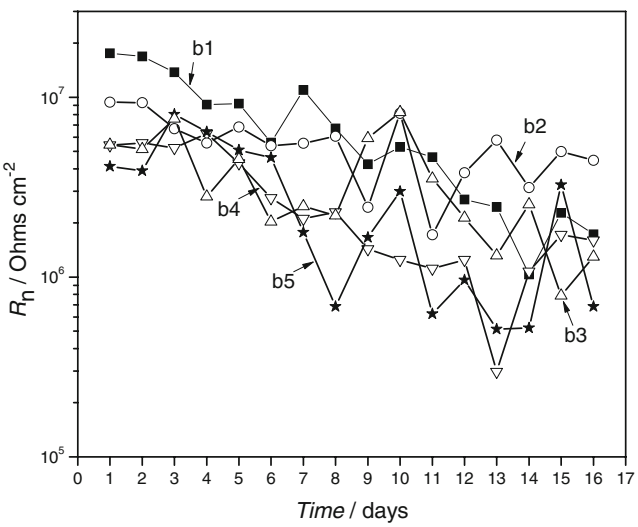

Fig. 8 Effect of Al content on the change in the noise resistance value with time, R_n, for Ni-AL-Fe intermetallic alloys in Hank's solution

Table 6 Localization index values for the different intermetallic alloys after 1 and 16 days of exposure to the Hank's solution

Material	Localization index	
	1day	16days
b1	0.91593	0.21427
b2	0.56675	0.17488
b3	0.95704	0.14320
b4	0.72946	0.23591
b5	0.94192	0.17849

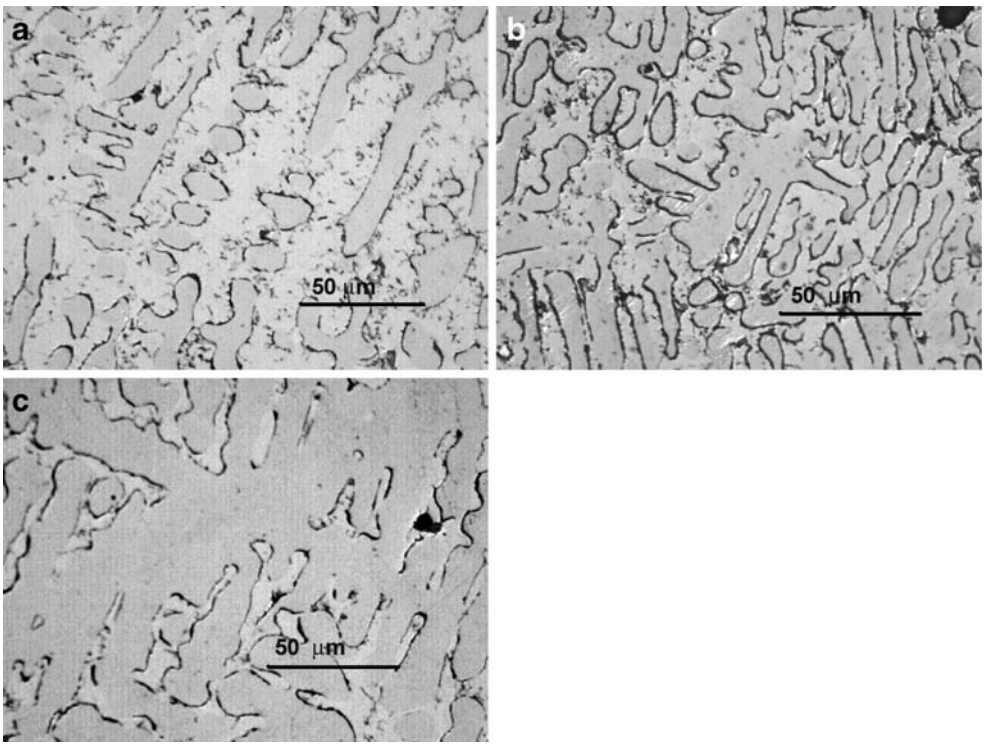

Fig. 9 Micrographs of Ni-AL-Fe alloys containing **a** 20, **b** 22.5, and **c** 25% Al exposed to the Hank's solution showing pitting type of corrosion in the interdendritic phases

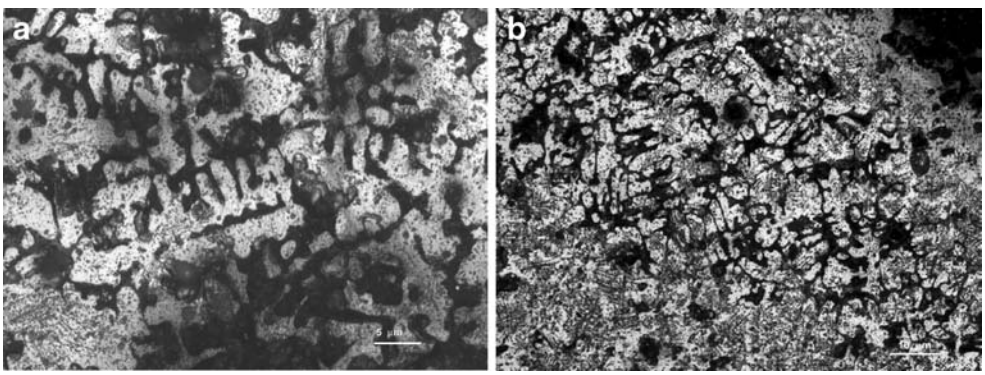

Fig. 10 Higher magnification of corroded Ni-AL-Fe alloys containing **a** 22.5, and **b** 25% Al showing interdendritic attack

susceptible to localized corrosion. Polarization curves have shown that Ni-Al-Fe intermetallic alloys could be passivated in human body environments. However, the erratic behavior in the R_p, R_n, and R_{ct} values has shown that this protective passive film can be detached from the surface, which was evidenced by Bode diagram on Fig. 5b, leaving the substrate unprotected against the corrosive environment. This film can be either in the whole surface or in some localized places, especially in presence of chlorides, allowing aggressive ions to attack the alloy in those points. Since the most susceptible phases, the interdendritic ones, acted as anodes, these were the preferential places for localized corrosion to occur. Normally, additions of Ni have been reported to increase the corrosion resistance of iron-base alloys in acidic solution, sea water, and alkaline solutions [19]. This corrosion resistance has been reported to be due to the establishment of a more stable passive layer. Frangini [20] has shown that additions of some ternary elements such as Cr or Ti to NiAl intermetallics improve the Al_2O_3 protectiveness by suppressing detachment of these scales. Additionally, they showed that, when Ni is added, the outwards diffusion of Ni will be faster than the inwards diffusion of Al, preventing the formation of voids on the surface which could lead to a scale detachment. In addition to this, by looking at the microstructures shown on Fig. 9, it can be observed that the average of the secondary dendrite arm spacing are 9 (±3 λm), 12 (±3 λm), and 17 (±3 λm) for Ni-20, 22.5, and 25 wt% Al alloys, respectively. Additionally, the Ni-25 wt% Al alloy has also evidenced ternary dendritic array. It can be observed that a coarser dendritic array (Ni-25 wt% Al alloy) has a lower interdendritic region than the other alloys, and, as a direct consequence, a better galvanic protection is provided. Since interdendritic region acted as a less noble region, it seems that a fine dendritic morphology is more susceptible to corrosion. The increased corrosion resistance has been reported to be due to the establishment of a more stable passive layer in addition to the formation of voids as explained above. If the relative contents of Ni into the passive layer decrease, by increasing the Al contents in the alloy, the improvement of the passive Al_2O_3 layer is loosened.

Conclusions

The corrosion behavior of Ni-Al-Fe intermetallic alloys as possible materials to be used in human body environments has been evaluated. Polarization curves have shown that, for short time tests, their corrosion resistance was lower than that for conventional AISI 316L type stainless steel, but they showed an active to passive behavior. Longer time tests such as linear polarization resistance and electrochemical noise measurements showed that these intermetallic alloys had a similar or even slightly better corrosion resistance than AISI 316L type stainless steel. This corrosion resistance decreased as the Al content in the alloy increased. The erratic change in the linear polarization resistance, R_p, and electrochemical noise resistance values, R_n, and the impedance modulus [Z] indicated that the passive film on the alloys could be detached from the surface inducing a localized, pitting type of corrosion in preferential places like interdendritic phases. EIS measurements showed that in alloys containing Al contents higher than 20%, the corrosion process was under charge transfer control, whereas for the most corrosion resistance, the alloy containing 20% Al, the corrosion process was under a mixed charge transfer and diffusion control.

References

1. Hallab N, Merritt K, Jacobs JJ (2001) J Bone and Joint Surgery 83:428
2. Choubey A, Basu B, Balasubramaniam R (2005) Trends Biomater Artif Organs 18:64
3. Sridhar TM, Mudali UK, Subbaiyan M (2003) Corros Sci 45:237
4. Zhou YL, Niinomi M, Akahori T, Fukui H, Toda H (2005) Mat Sci Eng 398A:28
5. Poon RWY, Ho JPY, Liu X, Chung CY (2005) Mat Sci Eng 390A:444
6. Cheng FT, Lo KH, Man HC (2007) J Alloys Compounds 437:322
7. Zheng YF, Wang BL, Wang JG, Li C, Zhao LC (2006) Mat Sci Eng 438A:891
8. Li YH, Rao GB, Rong LJ, Li YY, Ke W (2003) Mat Sci Eng 363A:356
9. Metikos-Hukovic M, Babic R (2007) Corros Sci 49:3570
10. Metikos-Hukovic M, Babic R (2009) Corros Sci 51:70
11. Clesic M, Reczyski W, Janus AM, Engvall K, Socha RP, Kotarba A (2009) Corros Sci 51:1157
12. Chern Lin JH, Chen KS, Ju CP (1995) Mat Chem Phys 41:282
13. Guo WY, Surr J, Wu JS (2008) Mat Chem Phys 113:616
14. Garcia-Alonso MC, Lopez MF, Escudero ML, Gonzalez-Carrasco JL, Morris DG (1999) Intermetallics 7:185
15. Lopez MF, Escudero ML, Vida E, Pierna AR, Marzo FF (1997) Electrochimica Acta 42:659
16. Lopez MF, Gutierrez A, Alonso-Garcia MC, Escudero ML (1998) J Mater Res 13:3144
17. Medvedeva NJ, Gornostyrev YN, Novikov DL, Myrasov ON, Freeman AJ (1998) Acta Metall Mater 46:3433
18. Albiter A, Espinosa-Medina MA, Gonzalez-Rodriguez JG (2004) J Appl Electrochem 34:1141
19. Zhou YL, Ninomi M, Akahori T, Fukui H, Toda H (2005) Mat Sci Eng 398A:28
20. Frangini S, Masci A (2004) Surf Coatings Technol 184:31
21. Martins DQ, Osorio WR, Souza MEP, Caram R, Garcia A (2008) Electrochim Acta 53:2809
22. Osorio WR, Cheung N, Spinelli JE, Goulart PR, Garcia A (2007) J Solid State Electrochem 11:1421
23. Assis SL, Wolynec S, Costa I (2006) Electrochim Acta 51:1815
24. Lee SJ, Pyun SI (2007) J Solid State Electrochem 11:829
25. Eden, D (1998) In: Corrosion '98 National Association of Corrosion Engineers, Houston, TX, 1998, paper no. 386